PAPER

Check for updates

High color rendering and high-luminance laser lighting using all inorganic nitride phosphor films

Zhi Jiang, [a] Shaoda Yuan,[a] Jian Xu,*[a] Baoli Du,[a] Peng Xu,[a] Le Zhang,*[bc]
Jian Kang, [bc] Yujie Zhao, [d] Carsten Dam-Hansen[e] and Ole Bjarlin Jensen[e]

Despite the huge advances that have been made in the development of ultra-high luminance laser lighting, achieving high color rendering properties in such systems at the same time remains a challenge. Recent studies show that in most cases, the luminous efficacy (LE) of laser lighting is compromised to improve the color rendering index (CRI). In this study, a possible solution to this problem has been proposed by preparing phosphor-in-glass (PiG) films comprised of the yellow-emitting phosphor (LSN:Ce^{3+}) and the red-emitting phosphor (CASN:Eu^{2+}). The composite material synthesized in this study exhibited outstanding optical and thermal properties. A uniform white light with a high CRI of 80.0 and a high LE of 185.9 lm W^{-1} was achieved by optimizing the yellow/red ratio and the emission peak position of the blue laser. Furthermore, it was found that this design enabled the phosphor to restrict the light emission area effectively, thus attaining a high luminous exitance of 1302 lm mm^{-2}. With their superior optical performance, the PiG films can be regarded as promising color converter candidates for future high-quality laser-based white light sources.

1. Introduction

Solid-state lighting technology, represented mainly by white light-emitting diodes (wLEDs) with long service lifespan and good color rending, is more energy efficient and eco-friendly than other lighting solutions.[1–5] It is gradually replacing the traditional lighting device with rapid economic development in many fields. However, "Efficiency droop", referring to the reduction of efficiency with increasing injection current density (input power) and temperature, seriously restricts the application of wLEDs in high power, high luminance, and high temperature applications.[6,7]

The laser diode (LD) technology, however, is not faced with the above-mentioned challenge as an LD can maintain a high wall-plug efficiency even at high input power densities. Additionally, LDs exhibit better properties such as higher photoluminescence quantum yields per chip area, higher optical output powers, and a more efficient secondary light emission process in comparison to LEDs.[8,9] Therefore, LDs are considered

[a] *School of Physics and Electronic Information, Henan Polytechnic University, Jiaozuo 454000, P. R. China. E-mail: xujian@hpu.edu.cn*

[b] *School of Physics and Electronics Engineering, Jiangsu Normal University, Xuzhou 221116, P. R. China*

[c] *Jiangsu Xiyi Advanced Materials Research Institute of Industrial Technology, Xuzhou 221400, P. R. China*

[d] *College of Physics and Engineering, Henan University of Science and Technology, Luoyang 471000, P. R. China*

[e] *Diode Lasers and LED Systems Group, Department of Electrical and Photonics Engineering, Technical University of Denmark, Roskilde 4000, Denmark*

more viable for the development of high-power white light sources to be used in applications such as car headlights, searchlights, and projectors.[10–12]

Similar to the phosphor-converted wLED, high-brightness laser-based white lighting is achieved by integrating blue LDs as an irradiation source with luminescent materials.[13] The LE, CRI, and thermal stability of laser lighting devices are mainly determined by the luminescent material and its packing method. However, with poor heat resistance and low thermal conductivity, the traditional LED packaging method, phosphor-in-silicone (PiS), will unavoidably lead to not only methyl yellowing, carbonization, and thermal failure, but also, thermal quenching of phosphor and the reduction of conversion efficiency under long-time irradiation of high-power laser.[14–17] So, new packing technology must be developed to avoid the inherent problems of PiS, including decline of the luminous efficacy, shift of chromaticity and correlated color temperature (CCT), and the decrease of long-term reliability when using in phosphor-converted white laser diode (pc-wLD).

In order to overcome its intrinsic problems, various inorganic color converters have been proposed and developed to replace the organic PiS, which include single crystals (SCs),[11,18] transparent ceramics (TCs)[19–21] and phosphor-in-glass (PiG)[22–24] converters. SCs offer clear advantages in terms of thermal stability and internal quantum efficiency (IQE). However, high-quality SCs are hard to fabricate and not available for many phosphors. Also, the elemental composition and doping level are difficult to regulate continually in SCs, making the optimization of luminosity and chromaticity across a wide range more

challenging.[18,25,26] In TCs, control of the absorption of light can be achieved by enhanced light scattering effects, which is much more convenient to be adjusted by internal microstructure manipulation than in SCs. Yet, the preparation of TCs requires a high vacuum environment when using nitride phosphors, and the unusually high coefficient of thermal expansion greatly increases the difficulty of preparing nitride transparent ceramics.[19–21] PiGs have simple preparation process, high transparency, and color tunability. Conventionally, the PiGs are generally thicker than 100 μm to guarantee sufficient absorption of laser irradiation. Due to the low thermal conductivity, its saturation threshold is low compared with SCs and TCs, which limits its application in high laser radiation power scenarios.[22–24]

To avoid the intrinsic disadvantage of low thermal conductivity and low saturation threshold, a PiG film (PiG-F) is developed by sintering a phosphor-glass film on a transparent or reflecting substrate, such as glass, sapphire, corundum or ceramic substrates.[27–29] In 2018, Xu et al. prepared YAG:Ce $(Y_3Al_5O_{12}:Ce^{3+})$/SiO$_2$ composite PiG film on a sapphire substrate.[27] No obvious luminous saturation occurs when the laser power density reaches 20.0 W mm^{-2} in PiG-F with a thickness of 50 μm. While inheriting the high color tunability of PiG, PiG-Fs avoid the tendency of thermal optical saturation by diffusing heat into substrates. Benefiting from the high heat diffusion ability of the substrate, the PiG-F packaging technology exhibits similar advantages of both TCs and PiGs. The preparation process of PiG-Fs is simple, with no secondary sintering and composite heat sink steps involved, and easy to be realized in industrial production.[29] The thickness of PiG-Fs is adjustable up to tens of μm by existing technology. Therefore, the flexible design of PiG-Fs can not only guarantee a high blue light absorption efficiency, but also a high saturation threshold, thus a tight bonding of film and substrate can be achieved.[30,31] For example, YAG:Ce PiG bears a maximum laser power density of only ~3.5 W mm^{-2}, much lower than the value reported in PiG-F.[32] The LSN:Ce $(La_3Si_6N_{11}:Ce^{3+})$-PiG shows a saturation threshold of just 5.5 W mm^{-2},[33] while the LSN:Ce PiG-F is capable of withstanding a laser power density as high as ~12.9 W mm^{-2}.[34] Both demonstrated the enormous potential of PiG-Fs in high brightness pc-wLD.

Even with these advancements, enhancing the CRI is crucial for further development, one of the primary reasons for the low CRI value obtained by PiG-F using a single phosphor is due to the laser blue peak having a full width at half maximum (FWHM) of less than 5 nm, which results in the limited coverage of the visible spectrum. The most popular commercially available yellow-emitting phosphor is YAG:Ce, which provides a CRI value of 73.0 at an excitation wavelength of 450 nm.[35] The spectral emission band of the YAG:Ce phosphor is also narrow, leaving much room for improvement in its color rendering index. In some previous studies, red emission was introduced by the addition of red-emitting ions such as Gd^{3+}, Gr^{3+} and Pr^{3+} in YAG:Ce.[36–39] Among them, the CRI value for Ce:GdYAG is slightly better than the other two candidates.[40] In the meantime, the yellow phosphor LSN:Ce that exhibits a wide spectral emission peak has a CRI value of just 74.9 after being

encapsulated as a PiG-F.[41] It is extremely difficult to obtain a high CRI value based on just a single phosphor under laser light illumination.

The use of two phosphors is a good and practical way to improve the CRI of pc-wLDs. The absence of red region in the spectrum is a huge constraint that limits further progress in the development of high-quality white light sources, as it is crucial to achieving a high CRI. A lot of research is being undertaken to produce a white light source with a high CRI. In 2018, Peng et al. fabricated a patterned CASN:Eu $(CaAlSiN_3:Eu^{2+})$ layer on a YAG:Ce PiG, which produced a CRI of 80.5, whereas its CCT reached up to 4831 K.[42] In 2020, Wu et al. used commercially available colloidal silica, CASN:Eu and LuAG:Ce to fabricate a composite film with a CRI of 92.0.[43] However, a low LE of 137.0 lm W^{-1} was obtained with poor adhesion to the glass matrix. In 2022, Hu et al.[44] fabricated a phosphor-in-glass film on a sapphire substrate using LuAG:Ce and CASN:Eu. A spatially homogeneous white light emission with an LF of 1408 lm and a CRI of 82.0 was achieved, but the LE was limited to a value of just 74.0 lm W^{-1}.[44]

As mentioned above, LSN:Ce exhibits many similarities with the YAG:Ce phosphor. However, LSN:Ce has a wider spectral emission band, in addition to exhibiting better thermal quenching performance than YAG:Ce.[34] These properties theoretically make LSN:Ce a more suitable candidate for laser lighting applications, as well as for the development of high-power LEDs and liquid crystal display (LCD) backlights. In addition, CASN:Eu is considered the most efficient red-light compensator due to its high IQE and its excellent thermal stability. It also adequately addresses the problem of low saturation threshold for laser lighting applications.[45,46]

PiG-F of the reflection configuration base was used to encapsulate both phosphors to reduce the effect of high laser radiation energy, thereby increasing the blue light absorption efficiency and at the same time improving the uniformity of the light source. The reflection configuration of the PiG-F is directly connected to the heat dissipation effect, which facilitates to control the working temperature of the lighting device accurately. It thereby provides a suitable working environment for the PiG-F to achieve excellent luminous efficacy in laser lighting devices with high-power density and ultra-high luminance.[29]

This work was focused on achieving improved color qualities, high saturation threshold, and high luminance of luminescent materials using LSN:Ce and CASN:Eu in the reflection configuration. The PiG-F was synthesized, and then the influence of different ratios of yellow/red phosphors was studied in detail. The two excitation wavelengths for the prepared PiG-F samples, their CRI values, saturation thresholds and luminescent spot sizes were hence obtained. The final optimized sample of LSN:Ce and CASN:Eu PiG-F exhibited a luminous saturation under laser illumination with a high power density of 18.0 W mm^{-2}, achieving a luminous efficacy reaching 185.9 lm W^{-1} and a CRI of 80.0. These results prove that the approach proposed in this work provides a perspective design for future high-quality laser lighting devices.

2. Materials and methods

2.1 Materials preparation

A viscous ink was synthesized by mixing a glass powder (SiO_2–Al_2O_3–B_2O_3–BaO–CaO, at $T_g \approx 425$ °C, $T_s \approx 500$ °C, Hunyuan Junhong), LSN:Ce powder (Beijing Grirem), CASN:Eu powder (Yantai Shield, SDR-630) and an organic vehicle. The mass of LSN phosphor and the glass powder was taken to be 0.8 g. The "CASN phosphor to LSN phosphor" weight ratio percentages were 20%, 10%,6.7%, 5%, 4% and 2%. The six prepared samples were named as PiG-F-5/1, PiG-F-10/1, PiG-F-15/1, PiG-F-20/1, PiG-F-25/1, and PiG-F-50/1. The viscous ink was printed onto a corundum (α-Al_2O_3, 99%) substrate (14 mm × 19 mm × 2 mm) using a screen-printing technique. For each sample, the printed layer was initially heated at a temperature of 120 °C for 3 h to remove all organic matter and then heated to a temperature of 510 °C with a ramp rate of 5 °C min^{-1} (the soaking time was zero).

2.2 Characterization

The X-ray diffraction (XRD) patterns of the PiG film were obtained using a Rigaku SmartLab (9 kW) X-ray diffractometer with Cu Kα radiation ($\lambda = 1.54056$ Å). The morphology of the PiG film was characterized by scanning electron microscopy (SEM, Carl Zeiss AG, Merlin Compact) coupled with energy-dispersive X-ray spectroscopy (EDS). Luminescence spectra were acquired using a HORIBA Fluorolog-3 spectrometer. The thermal quenching behavior was evaluated by using a spectroradiometer (Edinburgh Instruments, FLS-1000) equipped with a thermal stage.

The luminescence saturation behaviors were measured using a custom-made sphere-spectroradiometer system. The setup for high power density mode consists of a 3.5 W 441 nm LD (Nichia, NDB7A75) a 2 W 462 nm LD (M462), a fiber-coupled integrating sphere (Labsphere, RT-060-SF), and an array spectrometer (Instrument Systems, CAS-140-CT-151). Two separate lens systems consisting of a cylindrical lens ($f = 10$ mm), a cylindrical lens ($f = 150$ mm) and an achromatic lens ($f = 200$ mm) were used to shape and focus the light from the LDs. The laser beam profile was measured using a scanning slit beam profiler (Photon, Beamscan 2180). The output optical power of

the blue laser module was measured using a laser power meter (Ophir, NOVA-II). The spot size of the 441 nm laser module is ~0.12 mm^2. The spot size of the 462 nm laser module is ~0.09 mm^2. For measuring the size of the luminescent spot an additional setup was made.[47] The size of the blue laser beam spot along the beam direction was measured using a camera-based beam-profiler. By shifting the position of the laser system, it was possible to vary the laser spot size (e^{-2}) on the phosphor from 40 to 485 μm. To image the luminescent spot on the phosphor, a 4f imaging-system was used with a CMOS camera (Thorlabs, DCC1645C). Suitable long-pass filters were positioned between the phosphor and the camera to filter out the blue radiation, allowing only the luminescent spot to be imaged. A neutral density filter was also utilized to attenuate the light to avoid saturation of the camera.

3. Results and discussion

The XRD patterns of the prepared samples from PiG-F-5/1 to PiG-F-50/1 and the raw phosphor are presented in Fig. 1. It can be seen that the diffraction peaks for all samples correspond to the standard data of LSN:Ce (ICSD-248709) and CASN:Eu (PDF#39-0704). The strongest diffraction peaks (35.2°, 57.5°) of all samples comes from corundum. No impurity peaks were found in the samples. The results confirmed that the chemical properties of phosphor in the glass powder remained unchanged even under high temperatures that were used during the synthesis process. Hence, this proved that no chemical reaction between the phosphor and the glass powder took place and verified that the samples had successfully been synthesized. As the two phosphors that were used for the study both contained nitride groups, their corrosion properties were quite similar.

The granular morphology of pristine red-emitting phosphor CASN:Eu and yellow-emitting phosphor LSN:Ce particles is shown in Fig. 1(b) and (c). As shown in the figure, the two phosphor particles can clearly be seen. Both particles exhibit a relatively regular morphology in the shape of rod-like particles, with similar sizes as well. The maximum particle length was found to be about 20 μm. To obtain the distribution of the two particles in the PiG-F, the morphology of its surface and its cross-section were imaged using a scanning electron
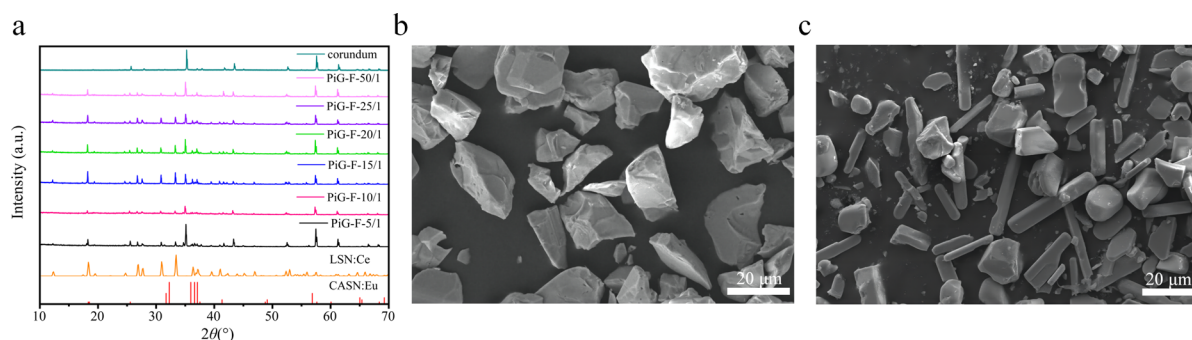

Fig. 1 (a) XRD patterns of LSN:Ce phosphor, CASN:Ce phosphor, PiG–F–5/1∼PiG–F–50/1, and the corundum substrate. SEM graphs of the commercial (b) LSN:Ce and (c) CASN:Eu pristine phosphors.
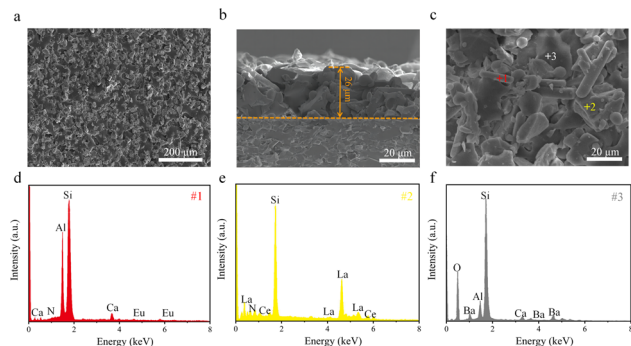
Fig. 2 (a) SEM images of the LSN&CASN PiG-F samples. (b) Cross-sectional SEM images of LSN&CASN PiG-F-5/1 samples. (c) SEM image showing points 1, 2 and 3 chosen for the elemental analysis. (d–f) EDS spectral analysis at points 1, 2 and 3 as indicated in (c).

microscope (SEM). As shown in Fig. 2(a), the glass was completely softened, and the entire surface of both particles was coated. It was also observed that the LSN:Ce and CASN:Eu particles were evenly distributed in the glass, forming a complete mesh-like structure along the sample surface without the formation of any large cracks or fractures. The SEM image showing the cross-sectional view of the LSN&CASN PiG-F is provided in Fig. 2(b). The image indicates that the phosphor had fused well with the glass powder, and that the film was bound strongly with the corundum substrate, without forming any large cracks at the substrate–film interface. According to the phosphor particle morphology shown in Fig. 1, three points were taken for the elemental composition analysis. Based on the shape of the two phosphor particles and the irregular morphology of the fused glass powder, the three points 1, 2, and 3 were selected as shown in Fig. 2(c). The results of the elemental distribution are presented in Fig. 2(d)–(f). By combining the known chemical composition of the three powders it was found that point 1 was CASN:Eu, point 2 was LSN:Ce, whereas point 3 was melted glass. The characteristic signatures of the other phosphor were not detected at points 1

and 2. Traces of the glass powder were found throughout the phosphor powders, owing to its uniform distribution.

To further confirm whether a reaction occurred at the glass–phosphor interface, an EDS mapping was performed. The results of this characterization are provided in Fig. 3(a)–(i). It can be seen that the rod-shaped phosphor particles were abundant in Al and Si elements. The distributions of the elements La and Ce were quite similar. However, neither of these two elements was found in the composition of the rod particle. The elements were non-uniformly distributed and scattered throughout the irregularly shaped fused glass. Also, there were no traces of the O element that were found at the more probable particle positions.

Based on the elemental distribution, it was observed that the boundary between the phosphor particles and the glass powder was quite clear. This confirmed that the chemical composition of pristine phosphor particles had not changed and no interface interaction between the phosphor particles and the glass took place. Individual particles were successfully embedded into the glass and its crystal structure remained unchanged. It can be seen that the pristine morphology of the phosphor was also preserved during the synthesis of PiG-F, as the two materials came into close contact with each other. This facilitated retaining the excellent luminescence properties of the phosphors such as the high IQE of the pristine powder.

The sample PiG-F-5/1 (with the largest proportion of red powder compared with other samples) was chosen first to be characterized by photoluminescence excitation (PLE). The results of this characterization are provided in Fig. 4(a). From exploration of the PL, the strongest emission peak was 528 nm. The detection monochromator of the PLE was set to 528 nm. The excitation spectrum of the PiG-F primarily corresponded to transitions from the $Ce^{3+}4f$ ($^2F_{5/2}$) ground state to its various 5d crystal-field levels. These transitions corresponded to light emissions in the near ultraviolet (350–420 nm) and blue (440–470 nm) spectral regions. Additionally, the PL spectra for the two pristine phosphors and their corresponding PiG-F samples are provided in Fig. 4(b) and (c), The results show that the PL characteristics of pristine phosphor were preserved only for the LSN:Ce PiG-F and the CASN:Eu PiG-F, which proves that the optical properties of pristine powder remained unaffected by the preparation of PiG-F.

All PiG-F samples were then characterized using photoluminescence spectroscopy (PL). The PL spectra of all PiG-F samples for the two excitation wavelengths of 441 nm and 462 nm are shown in Fig. 4(d) and (e). It can be observed that all samples have two emission bands, centered at 528 nm and 590 nm. The sharp emission peak at 528 nm can primarily be associated with the transition from $^2F_{5/2}$ levels in Ce^{3+} to its 5d orbitals.[34,48] The 590 nm red emission band formed as a result of the transition between the $4f^65d^1$ level in Eu^{2+} to its $4f^7$ level.[49] The results clearly show that the 590 nm emission peak is strongest in the intensity of the PiG-F-5/1 sample compared to all the other samples. By adjusting the weight ratio of the red and yellow phosphors, the overall trend of the PL under illumination by the two excitation wavelengths for all samples was consistent. Moreover, the FWHM was narrower for all samples.
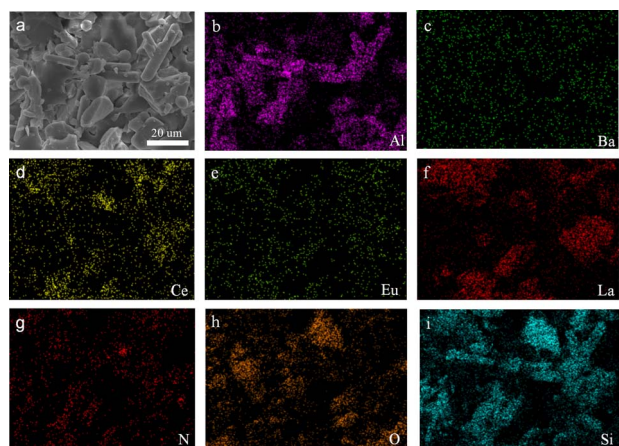

Fig. 3 (a) The SEM images of powder particles and (b–i) the related EDS mapping results of the PiG-F-5/1 sample surface.
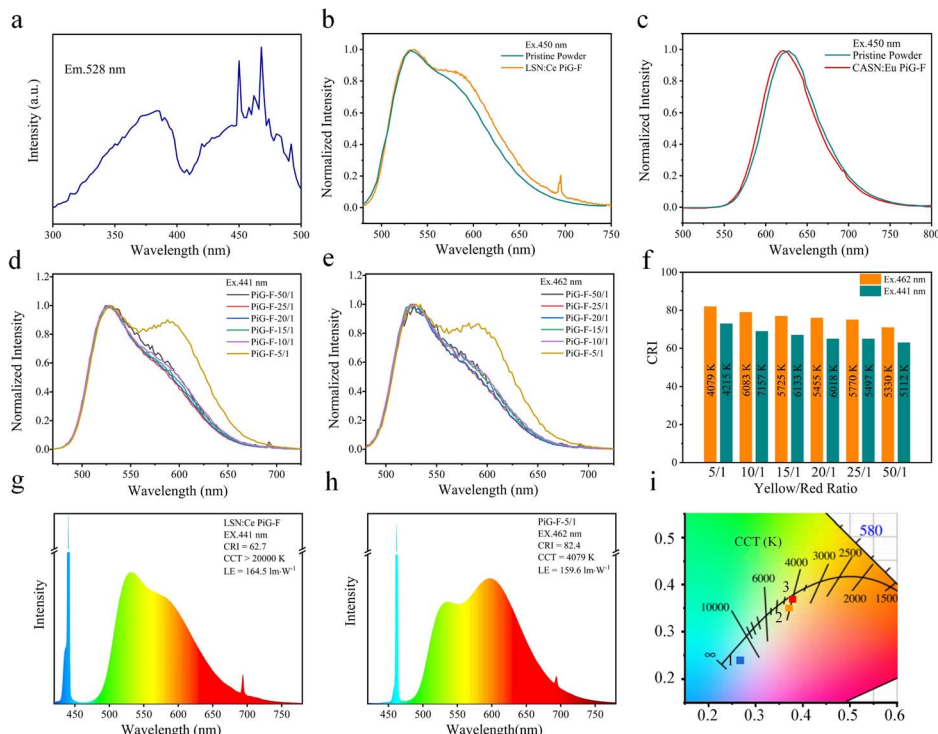
Fig. 4 (a) PLE spectra of PiG-F-5/1, PL spectra of (b) LSN:Ce PiG-F, LSN:Ce pristine powder and (c) CASN:Eu PiG-F, CASN:Eu pristine powder.[46] (d) The PL spectra of various samples pumped by the 441 nm and (e) 462 nm laser sources, respectively. (f) The obtained CRI and CCT values for different samples pumped by the 441 nm and 462 nm laser sources with various yellow to red phosphors ratios. (g) The EL spectra and optical properties for the LSN:Ce PiG-F pumped by the 441 nm laser source. (h) The EL spectra and optical properties for the PiG-F-5/1 sample pumped by the 462 nm laser source. (i) From points 1 to 3: CIE color coordinates for the LSN PiG-F pumped by 441 nm and the PiG-F-5/1 sample pumped by 441 nm and 462 nm laser sources, respectively.

To verify whether the composite PiG-F can be used as inorganic color converters for laser-based lighting and to study the effect of different excitation wavelength on the colorimetric and photometric parameters, two lasers (441 nm and 462 nm) were used. The CRI and CCT values for all samples (PiG-F-5/1-PiG-F-50/1) were obtained using 441 nm and 462 nm lasers with a fixed laser power of ~0.2 W. From Fig. 4(f) it could be seen that the average value of the CRI for all samples excited at 462 nm was 10 points higher than at 441 nm. The CRI of all samples decreased gradually as the ratio of yellow to red phosphor increased. Among them, the highest CRIvalue of 82.4 was observed for the PiG-F-5/1 sample upon excitation by the 462 nm laser source.

From the labeled CCT values, it can be inferred that change in CCT is not strongly dependent on the ratio of the two phosphors. The CCT value for the PiG-F-10/1 sample exceeded 6000 K, probably due to its surface micro-structure, leading to low absorption of blue light and hence resulting in a high CCT value. Nevertheless, it can be concluded that the CCT value of the PiG-F sample may be tuned by altering its micro-structure. Furthermore, the reason for the irregularity in CCT may also be due to the fact that LSN:Ce and CASN:Eu phosphors have different conversion efficiencies for blue light.

The spectrum of the LSN PiG-F under the illumination by 441 nm laser is presented in Fig. 4(g), whereas Fig. 4(h) shows

the spectrum of PiG-F-5/1 sample under 462 nm laser illumination.

It can be observed from Fig. 4(h) that in comparison to the single LSN PiG-F, the LSN&CASN composite film produced more regions of red emission. The CRI value increased from 62.7 to 82.4, achieving an improvement of approximately 31%. Additionally, the CCT significantly decreased from over 20 000 K to about 4000 K. It should be noted here that the CRI of the sample improved substantially, while its luminous efficacy just reduced from 164.5 lm W^{-1} to 159.6 lm W^{-1}. Hence an excellent compromise between the two parameters of CRI and LE was achieved. This is quite favorable for applications that require light sources with high luminance as well as high color rendering properties.

The color coordinates for LSN:Ce PiG-F are indicated by point 1 in Fig. 4(i), and the color coordinates for LSN&CASN PiG-F at 441 nm and 462 nm are indicated by points 2 and 3, respectively. Point 1 to 3 shifts the color coordinates from cold white light to warmer white light. As the laser wavelength shifts from 441 nm to 462 nm, the color coordinates (0.3755, 0.3686) move towards the black-body radiation curve. The above results prove that an excitation wavelength of 462 nm produces better results in comparison to the laser wavelength of 441 nm. Warmer white light with a high CRI and low CCT value is obtained upon excitation at the wavelength of 462 nm, because it

gives a better match to the reference light sources within the eye–sensitivity curve.

Further, the saturation characteristics of the composite PiG-F for specific laser lighting applications were studied. It was concluded from Fig. 4 that the use of 462 nm excitation wavelength can significantly enhance the optical properties of all the composite-coated samples. To further confirm whether the optical performance of the sample is related to the excitation wavelength, the 462 nm laser source was sharply focused (laser spot size ≈ 0.09 mm^2) onto the sample center. For better heat dissipation, thermally conducting glue was added between the sample and the heat exchanger. The capacity of the sample to withstand high laser power density was evaluated by this method.

Fig. 5(a) demonstrates that none of the prepared samples experienced luminous saturation as the laser power density increased with the available laser power. The LE of the PiG-F-20/1 sample shown in Fig. 5(b) reached a value of 187.4 lm W^{-1}. Among all samples, the values of LF and LE for the PiG-F-5/1 sample were the lowest. However, taking into account its high CRI, it is still quite promising from an application point of view in comparison to previous contenders.[50] The LE values for all samples initially increased and then dropped. This is most likely caused by a larger uncertainty in the measurement of laser power at low power, where a small offset will cause a large difference in LE. The phosphor should be most efficient at low power density, where there is no thermal quenching.

Most commercially available lasers operate at the wavelength of 440–450 nm. So, the values of LE and LF for all samples were obtained using the 441 nm laser under the same procedure, as described previously except that the laser spot size was ~0.12

mm^2. As shown in Fig. 5(d), the LF values for all samples increased as the laser power density increased. The PiG-F-25/1 sample can withstand the high power density of the laser. The maximum laser power density of 22.0 W mm^{-2} used in this work is much higher than previous studies.[43,51] The sample showed luminescence saturation under this power density. LF increased very slowly and CCT reaches 9800 K from the initial 5500 K.

The LF values obtained at the maximum power density were higher for the 441 nm laser source in comparison to the excitation by the wavelength of 462 nm. This is because the excited area at 441 nm is 33% larger, thus the PiG-F samples have more incident laser power when at the same power density. The results presented in Fig. 5(d) and (e) show no obvious relationship between the sample saturation threshold and the phosphor ratio, which actually depends on the microstructure of the specific sample. Given that all other controllable variables remain consistent, the only uncontrollable factor is the alteration in microstructure after annealing. However the PiG-F-5/1 shows the lowest saturation threshold, mainly attributed to the inferior thermal quenching performance of the CASN:Eu, which constitutes the highest proportion in the sample, making it susceptible to thermal luminescence saturation. As shown in Fig. 5(e), the trend of LE values as a function of the laser power density for all samples at the wavelength of 441 nm is quite similar to the trend that was obtained for the 462 nm laser source shown in Fig. 5(b). The LE for 462 nm excitation is higher than that for 441 nm, which might be because the phosphor conversion efficiency is similar but the photopic response from the residual blue light is higher for 462 nm (~40.0 lm W^{-1}) than for 441 nm (~27.0 lm W^{-1}).
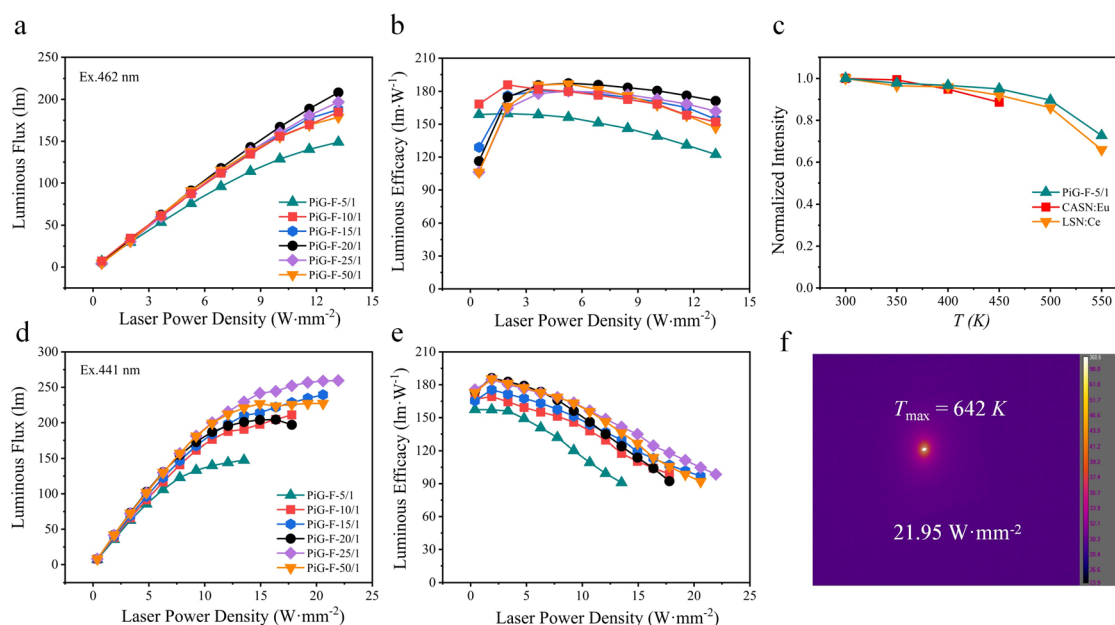

Fig. 5 The variation in the values of (a) LF and (b) LE as a function of laser power density for different samples pumped by the 462 nm laser source. (c) Temperature-dependent relative integrated emission intensity for LSN:Ce, CASN:Eu and PiG-F. The variation in the values of (d) LF and (e) LE as a function of the laser power density for different samples pumped by the 441 nm laser source. (f) Infrared thermal image of PiG-F-25/1 under laser illumination with a power density of 22.0 W mm^{-2}.
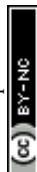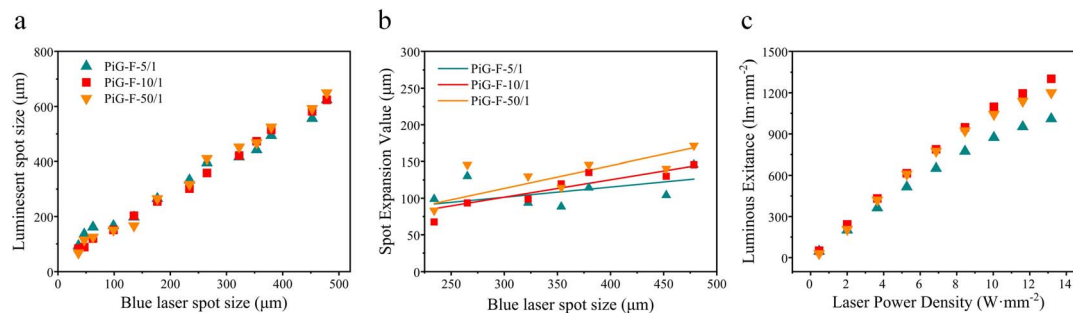

Fig. 6 (a) Spot size and (b) spot expansion for the PiG-F-5/1, PiG-F-10/1 and PiG-F-50/1 samples as a function of the laser spot size. (c) Luminous exitance for the PiG-F sample as a function of the laser power density under 462 nm laser excitation (the points are experimental data, and the corresponding line is linear regression).

The above results indicated that the composite samples displayed excellent optical properties. However, further investigation into the thermal saturations of the sample was needed. The results of the study on thermal quenching of LSN:Ce, CASN:Eu powder, and the PiG-F-5/1 sample are summarized in Fig. 5(c). As the operating temperature increased from 300 K to 550 K, the emission intensity of the PiG-F-5/1 sample was slightly lowered. This can be attributed to the thermal quenching effect caused by the non-radiative transitions, which is quite consistent with the pristine powder. As the operating temperature increased to 550 K, the PiG-F-5/1 sample was able to maintain 79% of its luminous intensity at room temperature, and the effect of thermal quenching remained minimal.

This indicated that the pristine phosphor was able to retain its inherent low thermal quenching property in the composite samples, and the annealing process did not induce any adverse effects on its thermal quenching properties.[52,53] Moreover, choosing a suitable glass cannot only avoid corrosion but also improve the thermal quenching properties of the PiG-F samples to a certain extent. Comparatively, this data shows promising results when compared to the widely-used YAG:Ce in practical applications. The overall thermal quenching ability of the samples was quite good. An infrared image for the central temperature of the spot at maximum laser power density is shown in Fig. 5(f) for PiG-F-25/1. Based on our experimental results, it was found that the use of a 462 nm excitation source has advantages over a 441 nm excitation source in terms of reducing the Stokes shift and minimizing energy loss, resulting in an improvement in thermal saturation performance. This finding is significant for the development and optimization of efficient fluorescent materials with high performance.

In addition to a high LF, developing a practical high luminance w-LD device requires control over the light emitting areas as well. Thus, the relationship between the laser spot size and the luminescent spot areas was also studied. The variation in the actual luminous spot size with the incident laser spot size for the three samples is shown in Fig. 6(a). The luminescent spot size for all tested samples increased linearly with increasing incident laser spot size. In case the total weight ratio of the phosphor to glass powder remains unchanged, a change in the yellow to red phosphor weight ratio can also be used to slightly affect the spots. This can primarily be associated with the two kinds of phosphor index sizes, which is consistent with previous studies (the ratio of the total mass of glass and phosphor on the influence of luminescent spot).[31] The plots for the spot expansion value (*i.e.*, the increase in the spot diameter) as a function of the incident laser spot size are shown in Fig. 6(b). As the laser spot size was increased, the expansion values for the PiG-F-5/1, PiG-F-10/1, and PiG-F-50/1 samples remained reasonably stable around the values of 95.2 μm, 87.2 μm, and 97.2 μm, respectively. Hence, this allowed to confine the spot size.

In addition to that, as the radius of the luminescent spot increased, the spot expansion value is relatively stable and the spot expansion area was reduced. If the laser spot size is known, the size of the ideal luminescent spot area required to realize controllable light emitting areas can be approximated. More importantly, the luminous exitance values for the PiG films were calculated based on the luminous spot sizes as measured in Fig. 6(a) and (b). As shown in Fig. 6(c), the luminous exitance of the PiG films increased almost linearly with increasing incident power density, which reaches a maximum merit of as high as 1302 lm mm^{-2} (the conversion to the luminance is 414 cd mm^{-2} assuming Lambertian emission). The results therefore clearly prove that all samples provided high luminance.

4. Conclusions

In summary, a series of LSN:Ce and CASN:Eu/glass composite films, exhibiting high color rendering properties, high luminance, and controllable emission areas is prepared. The composite PiG-F reaches a high CRI value of 80.0 upon excitation by a 462 nm blue LD, while still maintaining a high LE of about 185.9 lm W^{-1}, as required for applications by the lighting industry. The saturation threshold of the composite PiG-F is close to 18.0 W mm^{-2} as it is pumped by a 441 nm blue LD. At an operating temperature of 550 K, the luminous intensity of the PiG-F is reduced by just 21%, showing excellent thermal quenching properties. Moreover, this study proves that the PiG-F can confine the light emission area effectively. The above results hence provide sufficient evidence that this design produces a highly suitable luminescent material for obtaining high-quality white light and provides flexibility to tune various optical properties as well.

Author contributions

Jian Xu and Zhi Jiang contributed to the conception of the research. The design of the experiments took shape with input from Zhi Jiang. Zhi Jiang, Carsten Dam-Hansen and Ole Bjarlin Jensen performed the experiments and measurement. Zhi Jiang, Jian Xu and Baoli Du prepared the draft of the manuscript. Ole Bjarlin Jensen, Yujie Zhao and Le Zhang contributed significantly to the analysis. Shaoda Yuan helped to correct the mistakes in the paper. Le Zhang, Peng Xu and Jian Kang helped draft the manuscript with constructive discussions. All authors assisted in the editing of the final manuscript.

Conflicts of interest

There are no conflicts to declare.

Acknowledgements

References

1 Y. Wei, G. Xing, K. Liu, G.-G. Li, P.-P. Dang, S.-S. Liang, M. Liu, Z.-Y. Cheng, D. Jin and J. Lin, New strategy for designing orangish-red-emitting phosphor via oxygen-vacancy-induced electronic localization, *Light: Sci. Appl.*, 2019, **8**, 15.

2 S. Tim and R. J. A. van Dijk-Moes, Quenching of the red Mn^{4+} luminescence in Mn^{4+}-doped fluoride LED phosphors, *Light: Sci. Appl.*, 2018, **7**, 8.

3 P.-P. Dai, C. Li, X. T. Zhang, J. Xu, X. Chen, X. L. Wang, Y. Jia, X. J. Wang and Y. C. Liu, A single Eu^{2+}-activated high-color-rendering oxychloride white-light phosphor for white-light-emitting diodes, *Light: Sci. Appl.*, 2016, **5**, e16024.

4 Y. Liu, X. Zhang, Z. D. Hao, Y. S. Luo, X. J. Wang and J. H. Zhang, Generating yellow and red emissions by co-doping Mn^{2+} to substitute for Ca^{2+} and Sc^{3+} sites in $Ca_3Sc_2Si_3O_{12}:Ce^{3+}$ green emitting phosphor for white LED applications, *J. Mater. Chem. C*, 2011, **21**, 16379–16384.

5 R. Haitz and J. Y. Tsao, Solid-state lighting: 'The case' 10 years after and future prospects, *Phys. Status Solidi A*, 2011, **208**, 17–29.

6 M.-H. Kim, M. F. Schubert, Q. Dai, J. K. Kim, E. F. Schubert, J. Piprek and Y. Park, Origin of efficiency droop in GaN-based light-emitting diodes, *Appl. Phys. Lett.*, 2007, **91**, 183507.

7 M. H. Crawford, LEDs for solid-state lighting: performance challenges and recent advances, *IEEE J. Sel. Top. Quantum Electron.*, 2009, **15**, 1028–1040.

8 J. J. Wierer, J. Y. Tsao and D. S. Sizov, Comparison between blue lasers and light-emitting diodes for future solid-state lighting, *Laser Photonics Rev.*, 2013, **7**, 963–993.

9 J. J. Wierer and J. Y. Tsao, Advantages of III-nitride laser diodes in solid-state lighting, *Phys. Status Solidi A*, 2015, **212**, 980–985.

10 S. Masui, T. Yamamoto and S. -I. Nagahama, A white light source excited by laser diodes, *Electron. Commun. Jpn.*, 2015, **98**, 23–27.

11 M. Cantore, N. Pfaff, R. M. Farrell, J. S. Speck, S. Nakamura and S. P. Denbaars, High luminous flux from single crystal phosphor-converted laser-based white lighting system, *Opt. Express*, 2016, **24**, A215–A221.

12 Y. Ma and X. B. Luo, Packaging for laser-based white lighting: Status and perspectives, *J. Electron. Packag.*, 2020, **142**, 010801.

13 J. Jargus, J. Vitasek, J. Nedoma, V. Vasinek and R. Martinek, Effect of selected luminescent layers on CCT, CRI, and response times, *Materials*, 2019, **12**, 2095.

14 J. S. Kim, O. H. Kwon, J. W. Jang, S. H. Lee, S. J. Han, J. H. Lee and Y. S. Cho, Long-term stable, low-temperature remote silicate phosphor thick films printed on a glass substrate, *ACS Comb. Sci.*, 2015, **17**, 234–238.

15 M. Oishi, S. Shiomi, T. Yamamoto, T. Ueki, Y. Kai, Y. Chichibu, S. F. Chichibu, A. Takatori and K. Kojima, High temperature degradation mechanism of a red phosphor, $CaAlSiN_3:Eu$ for solid-state lighting, *J. Appl. Phys.*, 2017, **122**, 113104.

16 X. R. Ding, M. Li, Z. T. Li, Y. Tang, Y. X. Xie, X. T. Tang and T. Fu, Thermal and optical investigations of a laser-driven phosphor converter coated on a heat pipe, *Appl. Therm. Eng.*, 2019, **148**, 1099–1106.

17 S. S. Lin, H. Lin, G. X. Chen, B. Wang, X. M. Yue, Q. G. Huang, J. Xu, Y. Cheng and Y. S. Wang, Stable CsPbBr3-glass nanocomposite for low-étendue wide-color-gamut laser-driven projection display, *Laser Photonics Rev.*, 2021, **15**, 2100044.

18 K. W. Park, S. G. Lim, G. Deressa, J. S. Kim, T. W. Kang, H. L. Choi, Y. M. Yu, Y. S. Kim, J. G. Ryu, S. H. Lee and T. H. Kim, High power and temperature luminescence of $Y_3Al_5O_{12}:Ce^{3+}$ bulky and pulverized single crystal phosphors by a floating-zone method, *J. Lumin.*, 2015, **168**, 334–338.

19 Q. Du, S. Feng, H. Qin, H. Hua, H. Ding, L. Jia, Z. Zhang, J. Jiang and H. Jiang, Massive red-shifting of Ce^{3+} emission by Mg^{2+} and Si^{4+} doping of YAG:Ce transparent ceramic phosphors, *J. Mater. Chem. C*, 2018, **6**, 12200–12205.

20 S. Li, Q. Zhu, D. Tang, X. Liu, G. Ouyang, L. Cao, N. Hirosaki, T. Nishimura, Z. Huang and R.-J. Xie, Al_2O_3-YAG:Ce composite phosphor ceramic: a thermally robust and efficient color converter for solid state laser lighting, *J. Mater. Chem. C*, 2016, **4**, 8648–8654.

21 X. Liu, X. l. Qian, Z. W. Hu, X. P. Chen, Y. Shi, J. Zou and J. Li, Al_2O_3-Ce:GdYAG composite ceramic phosphors for high-

power white light-emitting-diode applications, *J. Eur. Ceram. Soc.*, 2019, **39**, 2149–2154.

22 K. Han, S. H. Lee, Y. G. Choi, W. B. Im and W. J. Chung, Improved color rendering index and thermal stability of white LEDs with phosphor-in-glass using the SiO$_2$-B$_2$O$_3$-ZnO-Na$_2$O glass system, *J. Non-Cryst. Solids*, 2016, **445**, 77–80.

23 Q.-Q. Zhu, X. Xu, L. Wang, Z. F. Tian, Y. Z. Xu, N. Hirosaki and R.-J. Xie, A robust red-emitting phosphor-in-glass (PiG) for use in white lighting sources pumped by blue laser diodes, J. Alloys. Compd, *J. Alloys Compd.*, 2017, **702**, 193–198.

24 X. Zhang, J. Yu, J. Wang, B. Lei, Y. Liu, Y. Cho, R.-J. Xie, H.-W. Zhang, Y. Li, Z. Tian, Y. Li and Q. Su, All-inorganic light convertor based on phosphor-in-glass engineering for next-generation modular high-brightness white LEDs/LDs, *ACS Photonics*, 2017, **4**, 986–995.

25 S. Arjoca, E. G. Víllora, D. Inomata, K. Aoki, Y. Sugahara and K. Shimamura, Ce:(Y$_{1-x}$Lu$_x$)$_3$Al$_5$O$_{12}$ single-crystal phosphor plates for high-brightness white leds/lds with high-color rendering (Ra > 90) and temperature stability, *Mater. Res. Express*, 2014, **1**, 025041.

26 Q. L. Sai, Z. W. Zhao, C. T. Xia, X. D. Xu, F. Wu, J. Q. Di and L. L. Wang, Ce-doped Al$_2$O$_3$-YAG eutectic and its application for white LEDs, *Opt. Mater.*, 2013, **35**, 2155–2159.

27 J. Xu, B. G. Liu, Z. W. Liu, Y. X. Gong, B. F. Hu, J. Wang, H. Li, X. L. Wang and B. L. Du, Design of laser-driven SiO$_2$-YAG:Ce composite thick film: Facile synthesis, robust thermal performance, and application in solid-state laser lighting, *Opt. Mater.*, 2018, **75**, 508–512.

28 J. Xu, Y. Yang, Z. Q. Guo, B. F. Hu, J. Wang, B. L. Du, B. G. Liu, H. P. Ji, C. Dam-Hansen and O. B. Jensen, Design of a CaAlSiN$_3$:Eu/glass composite film: Facile synthesis, high saturation-threshold and application in high-power laser lighting, *J. Eur. Ceram. Soc.*, 2020, **40**, 4704–4708.

29 J. Xu, Y. Yang, J. Wang, B. L. Du, A. A. Santamarí, B. F. Hu, B. G. Liu, H. P. Ji, C. D. Hansen and O. B. Jensen, Industry-friendly synthesis and high saturation threshold of a LuAG:Ce/glass composite film realizing high-brightness laser lighting, *J. Eur. Ceram. Soc.*, 2020, **40**, 6031–6036.

30 X. J. Zhang, S. C. Si, J. B. Yu, Z. J. Wang, R. H. Zhang, B. F. Lei, Y. L. Liu, J. L. Zhuang, C. F. Hu, Y. J. Cho, R.-J. Xie, H.-W. Zhang, Z. F. Tian and J. Wang, Improving the luminous efficacy and resistance to blue laser irradiation of phosphor-in-glass based solid state laser lighting through employing dual-functional sapphire plate, *J. Mater. Chem. C*, 2019, **7**, 354–361.

31 J. Xu, L. J. Wang, W. Gu, Z. Jiang, X. R. Chen, B. F. Hu, B. L. Du, H. P. Ji, C. D. Hansen and O. B. Jensen, Emitting area limitation via scattering control in phosphor film realizing high-luminance laser lighting, *J. Eur. Ceram. Soc.*, 2022, **42**, 608–615.

32 D. Zhang, W. G. Xiao, C. Liu, X. F. Liu, J. J. Ren, B. B. Xu and J. R. Qiu, Highly efficient phosphor-glass composites by pressureless sintering, *Nat. Commun.*, 2020, **11**, 2805.

33 P. Sui, H. Lin, Y. Lin, S. S. Lin, J. J. Huang, J. Xu, Y. Cheng and Y. S. Wang, Toward high-power-density laser-driven lighting:

34 enhancing heat dissipation in phosphor-in-glass film by introducing h-BN, *Opt. Lett.*, 2022, **47**, 3455–3458.

34 S. H. You, S. X. Li, P. Zheng, T. L. Zhou, L. Wang, L. H. Liu, N. Horisaki, F. F. Xu and R.-J. Xie, A Thermally Robust La$_3$Si$_6$N$_{11}$:Ce-in-Glass Film for High-Brightness Blue-Laser-Driven Solid State Lighting, *Laser Photonics Rev.*, 2019, **13**, 1800216.

35 R. Wei, L. Wang, P. Zheng, H. T. Zeng, G. M. Pan, H. Zhang, P. Liang, T. L. Zhou and R.-J. Xie, On the luminance saturation of phosphor-in-glass (PiG) films for blue-laser-driven white lighting: Effects of the phosphor content and the film thickness, *J. Eur. Ceram. Soc.*, 2019, **39**, 1909–1917.

36 S. Nishiura, S. Tanabe, K. Fujioka and Y. Fujimoto, Transparent Ce^{3+}:GdYAG ceramic phosphors for white LED, *Proc. SPIE*, 2011, **7934**, 18–23.

37 J. Huang, Y. R. Ni, Y. L. Ma, Y. B. Li, Z. X. Sun, X. Y. Zhu, R. Wang, T. Li, X. Q. Xi, G. C. Huang, T. Y. Zhou, M. Li, H. D. Ren, L. Zhang and H. Chen, Composite structure Cr:YAG/Ce:YAG and (Ce, Cr):YAG/Ce:YAG transparent ceramics with high color rendering index for white LEDs/LDs, *Ceram. Int.*, 2021, **47**, 11415–11422.

38 Y. R. Tang, S. M. Zhou, X. Z. Yi, S. Zhang, D. M. Hao and X. C. Shao, The Cr-doping effect on white light emitting properties of Ce:YAG phosphor ceramics, *J. Am. Ceram. Soc.*, 2017, **100**, 2590–2595.

39 Y. R. Tang, S. M. Zhou, X. Z. Yi, D. M. Hao, X. C. Shao and J. Chen, The characterization of Ce/Pr-doped YAG phosphor ceramic for the white LEDs, *J. Alloys Compd.*, 2018, **745**, 84–89.

40 L. H. Wang, J. D. Zhang, L. Xu, S. Y. Bao, Y. Wang, J. W. Liu, X. J. Liang and W. D. Xiang, Ce:GdYAG phosphor-in-glass: An innovative yellow-emitting color converter for solid-state laser lighting, *J. Mater. Sci. Technol.*, 2023, **134**, 42–49.

41 M. H. Huang, Q. Q. Zhu, Y. Meng, X. Y. Hu, H. Zhang and L. Wang, Synthesis and Performance of La$_3$Si$_6$N$_{11}$:Ce^{3+} Phosphor-in-glass Films for Laser Lighting Applications, *Chinese. J. Lumin.*, 2021, **42**, 1482–1492.

42 Y. Peng, Y. Mou, X. Guo, X. J. Xu, H. Li, M. X. Chen and X. B. Luo, Flexible fabrication of a patterned red phosphor layer on a YAG:Ce^{3+} phosphor-in-glass for high-power WLEDs, *Opt. Mater. Express*, 2018, **8**, 605–614.

43 H. J. Wu, Z. D. Hao, G.-H. Pana, L. L. Zhang, H. Wu, X. Zhang, L. G. Zhang and J. H. Zhang, Phosphor-SiO$_2$ composite films suitable for white laser lighting with excellent color rendering, *J. Eur. Ceram. Soc.*, 2020, **40**, 2439–2444.

44 Q. G. Huang, P. Sui, F. Huang, H. Lin, B. Wang, S. S. Lin, P. F. Wang, J. Xu, Y. Cheng and Y. S. Wang, Toward High-Quality Laser-Driven Lightings: Chromaticity-Tunable Phosphor-in-Glass Film with "Phosphor Pattern" Design, *Laser Photonics Rev.*, 2022, **16**, 2200040.

45 S. B. Kwon, B. Y. Kim, S. H. Choi, J. H. Yoo, W. H. Kim, J. P. Kim, H. J. Jeong, D. J. Park, B. K. Kang, D. H. Yoon and Y. H. Song, Fabrication of red-emitting CaAlSiN$_3$:Eu^{2+} through phosphor-in-glass approach for application in rear combination lamp, *Curr. Appl. Phys.*, 2020, **20**, 1281–1287.

46 J. Xu, Y. Yang, Z. Jiang, B. F. Hu, X. L. Wang, H. P. Ji, J. Wang, Z. Q. Guo, B. L. Du, C. D. Hansen d and O. B. Jensen, CaAlSiN$_3$:Eu/glass composite film in reflective configuration: A thermally robust and efficient red-emitting color converter with high saturation threshold for high-power high color rendering laser lighting, *Ceram. Int.*, 2021, **47**, 15307–15312.

47 A. Krasnoshchoka, A. K. Hansen, A. Thorseth, D. Marti, P. M. Petersen, J. Xu and O. B. Jensen, Phosphor material dependent spot size limitations in laser lighting, *Opt. Express*, 2020, **28**, 5758–5767.

48 F. Du, W. D. Zhuang, R. H. Liu, Y. H. Liu, W. Gao, X. Zhang, Y. Xue and H. R. Hao, Synthesis, structure and luminescent properties of yellow phosphor La$_3$Si$_6$N$_{11}$:Ce^{3+} for high power white-LEDs, *J. Rare Earths*, 2017, **35**, 1059–1064.

49 S. X. Li, Q. Q. Zhu, L. Wang, D. M. Tang, Y. J. Cho, X. J. Liu, N. Hirosaki, T. Nishimura, T. Sekiguchi, Z. R. Huang and R. J. Xie, CaAlSiN$_3$:Eu^{2+} translucent ceramic: a promising robust and efficient red color converter for solid state laser displays and lighting, *J. Mater. Chem. C*, 2016, **4**, 8197–8205.

50 Y. Mou, J. Z. Zhao, Z. K. Yu, Q. Wang, M. X. Chen and Y. Peng, Highly reflective interface design for phosphor-in-glass converter enabling ultrahigh efficiency laser-driven white lighting, *J. Eur. Ceram. Soc.*, 2022, **42**, 7579–7586.

51 P. Zheng, S. X. Li, L. Wang, T. L. Zhou, S. H. You, T. Takeda, N. Hirosaki and R. J. Xie, Unique color converter architecture enabling phosphor-in-glass (PiG) films suitable for high-power and high-luminance laser-driven white lighting, *ACS Appl. Mater. Interfaces*, 2018, **10**, 14930–14940.

52 P. Du, W. G. Ran, Y. F. Hou, L. H. Luo and W. P. Li, Eu^{3+}-activated NaGdF$_4$ nanorods for near-ultraviolet light-triggered indoor illumination, *ACS Appl. Nano Mater.*, 2019, **2**, 4275–4285.

53 P. Du, W. G. Ran, W. P. Li, L. H. Luo and X. Y. Huang, Morphology evolution of Eu3+-activated NaTbF4 nanorods: a highly-efficient near-ultraviolet light-triggered red-emitting platform towards application in white light-emitting diodes, *J. Mater. Chem. C*, 2019, **7**, 10802–10809.